5-1-2015

Mechanisms of Cell Cycle Delay and Death in Stathmin Depleted p53-Deficient Cells

Arianna Caruso
Lehigh University

Mechanisms of Cell Cycle Delay and Death in Stathmin Depleted p53-Deficient Cells

Arianna Caruso
Advisor: Dr. Lynne Cassimeris
2015

Introduction:

An essential component of cellular function is the integration of numerous signals to generate a single response. For example, every cell receives multiple intrinsic and extrinsic cues that influence whether or not it will survive or undergo the process of programmed cell death, known as apoptosis. In short, alterations in signaling may influence cell fate. The question then arises: What signals tip the balance towards cell death as opposed to cell survival? We are interested in the role of the microtubule cytoskeleton and its accessory proteins in the survival of cancer cells. Thus, we have narrowed this question to ask what is the role of microtubule regulatory proteins in tipping the balance toward cancer cell death?

Microtubules are hollow filaments approximately 25nm in diameter that are composed of α/β-tubulin heterodimers (2). During microtubule nucleation, α/β-tubulin heterodimers polymerize in a polarized fashion and form linear chains known as protofilaments (2). Thirteen protofilaments arrange in parallel to form sheets that are held together by non-covalent lateral and longitudinal bonds (2). These sheets subsequently circularize to complete the tube-like structure (2). An important component of microtubule nucleation is the γ-tubulin ring complex (2). The γ-tubulin ring complex has a helical pitch that matches that of a microtubule (2). Further, the γ-tubulin ring complex binds the α-tubulin face of a α/β-tubulin heterodimer to initiate microtubule nucleation (2). As a result, the localization of γ-tubulin ring complexes spatially controls microtubule nucleation (9).

The site at which microtubule polymerization occurs is known as a microtubule-organizing center (9). The main microtubule-organizing center in a cell is the centrosome (9). The centrosome is composed of two centrioles and is surrounded by the pericentriolar matrix, which contains proteins that specialize in γ-tubulin recruitment (9). Microtubules that arise from

the centrosome radiate outwards towards the cell periphery, and are essential in the formation of the mitotic spindle (9). Thus, microtubules play a pivotal role in cell division.

Many frequently used chemotherapy drugs, such as paclitaxel and vinblastine, are thought to cause cell death by interrupting microtubule spindle formation and consequently activating a cell cycle checkpoint (1). Of recent interest are microtubule regulatory proteins, which may also provide useful targets for cancer therapy. The microtubule regulatory protein stathmin/Oncoprotein 18 is overexpressed in many highly malignant cancers such as leukemia, lymphoma, prostrate cancer, and breast cancer (1). Stathmin sequesters free α/β-tubulin heterodimers and promotes depolymerization (2). There is evidence that stathmin is specifically required for the survival of p53-deficient cells (1). Notably, p53 is a tumor suppressor gene that is deficient in over 50% of cancer cells (1). The primary role of p53 is to temporarily halt cell proliferation or activate apoptosis in response to DNA damage (2). Cells lacking p53 are less efficient at repairing damaged DNA and activating apoptosis in the event that the damage is beyond repair (2). Depletion of stathmin in p53-deficient cells results in a ~4 hour delay in mitotic entry and ultimately increases the amount of cell death via activation of the extrinsic apoptotic pathway (11; 12) (Figure 2A).

With regards to the delay in mitotic entry, there is evidence that stathmin regulates mitotic entry in part by controlling the activation and localization of the mitotic enzymes Aurora A Kinase (AURKA) and Plk1 (11). AURKA and Plk1 have been shown to regulate microtubule nucleation and assembly on centrosomes (11). Both enzymes are involved in a positive feedback loop with CDC25 that results in the activation of CDK1/cyclin B (11). Sufficient activation of CDK1/cyclin B allows cells to overcome the restriction point in the cell cycle and ensures

commitment to mitosis (2). Stathmin depletion delays localization of AURKA and Plk1 to the centrosome and subsequently inhibits their activation (11).

With regards to cell death, p53-deficient cells exhibit low expression of cFLIP, a protein that blocks caspase-8 activation (12). The level of cFLIP is further reduced by stathmin depletion (12). This ultimately results in the activation of caspase 8 (12). Activated caspase 8 ultimately increases the cells' propensity towards death via the extrinsic apoptotic pathway (12).

Despite much advancement, there is still a lot that is unknown regarding the phenotype of stathmin depleted p53-deficient cells. The following models propose mechanisms for the delayed mitotic entry and increase in cell death, respectively.

The first proposed model addresses the delay in mitotic entry. This model links microtubule regulation and the Golgi apparatus. The Golgi apparatus is a critical component in the eukaryotic secretory pathway and is essential for the sorting and packaging of newly formed proteins (13). Notably, the Golgi apparatus is composed of multiple flattened, membrane bound structures known as cisternae, which are organized into parallel arrays to form individual stack structures (13). In eukaryotic cells, multiples of these stack structures are linked together to form a continual membrane known as the Golgi ribbon, which is localized adjacent to the centrosome (13). Recently, it has been found that the components in the pericentriolar matrix that recruit γ-tubulin to the centrosome also recruit γ-tubulin to the Golgi apparatus (10). For example, it has been shown that AKAP450, a γ-tubulin ring complex interacting protein that is localized at the centrosome, recruits γ-tubulin to the Golgi by binding to the cis-Golgi matrix protein GM130 (10). As a result, there is now evidence that the Golgi apparatus is a site of microtubule nucleation (10). Like for the centrosome, it has been demonstrated that Golgi nucleated microtubules are anchored by dynein and dynactin protein complexes (10). It has since been

suggested that Golgi nucleated microtubules are essential for maintaining the integrity of the ribbon structure (9). Importantly, in vertebrates, fragmentation of the Golgi ribbon prior to mitotic entry is essential to promote equal distribution of the Golgi between daughter cells (4). During this process, the Golgi ribbon is unlinked into individual subunits, and subsequently unstacked into individual cisternae (9). Following cytokinesis, the cisternae reassemble into a continual ribbon structure (9). Research has shown that blocking the unlinking of the Golgi ribbon in G2 causes a delay in mitotic entry (14). Further, there is evidence that blocking Golgi dispersal impairs the localization and activation of AURKA at the centrosome (7). We suggest that stathmin regulates microtubules at the Golgi, as well as the centrosome. Following this postulation, we predict that stathmin depletion stabilizes Golgi nucleated microtubules, thus preventing Golgi dispersal and delaying mitotic entry (Figure 1A).

To address the proposed model we first raise the question, does stathmin depletion in p53-deficient cells effect dispersal of the Golgi apparatus? In order to examine this question, we have utilized an artificial assay to trigger Golgi dispersal in stathmin depleted p53-deficient cells. We hypothesized that stathmin depletion stabilizes Golgi nucleated microtubules and ultimately slows Golgi fragmentation and dispersal.

The second proposed model addresses the increase in cell death. This model links microtubule regulation to a signal transduction pathway. It has been suggested that stathmin is involved in a negative feedback loop with c-Jun N-terminal kinase (JNK) (15). Specifically, oxidative stress, and the resulting accumulation of reactive oxygen species, triggers the phosphorylation of MKK-4, which in turn activates JNK through a phosphorylation event (15). Active JNK subsequently inactivates stathmin by phosphorylation at Ser-16, Ser-25, and Ser-38. Phosphorylated stathmin in turn inhibits the activation of MKK-4 (15). This negative feedback

loop promotes cell survival (15). Without this feedback loop, there is prolonged activation of JNK, which stimulates apoptosis (15). One way that active JNK has been shown to induce apoptosis is by increasing the degradation of cellular FLICE-like inhibitory protein (c-FLIP) (3). Specifically, active JNK activates the E3 ubiquitin ligase ITCH by phosphorylation (3). Activated ITCH subsequently ubiquitinates c-FLIP, thus triggering proteasomal degradation of c-FLIP (3). Degradation of c-FLIP promotes cleavage of pro-caspase-8 to form active caspase-8 (2). This results in the initiation of the extrinsic apoptotic pathway (2). As previously mentioned, stathmin depleted p53-deficient cells have significantly reduced levels of c-FLIP, which is in part responsible for the increase in cell death seen via the extrinsic apoptotic pathway (13). We suggest that stathmin depletion in p53-deficient cells results in prolonged activation of JNK, which in turn activates ITCH causing the degradation of c-FLIP and cell death via caspase-8 (Figure 2B).

To address this proposed model we examined the effect of stathmin and ITCH double depletion in p53-deficient cells. We hypothesized that depletion of ITCH in stathmin depleted cells restores cell viability. Specifically, if stathmin depletion increases ITCH activation but ITCH is depleted, than there will be minimal ITCH activity. Thus, there should be less c-FLIP degradation and less death via the extrinsic apoptotic pathway.

Overall, this work seeks to identify the mechanisms by which stathmin depletion in p53-deficient cells leads to delayed mitotic entry and cell death by testing the models outlined above. Doing so may play a pivotal role in identifying stathmin as a potential therapeutic target.

Materials/Methods:

Cell Culture:

Hela cells were grown and maintained at 37°C in a humidified environment consisting of 5% CO_2. The media used to culture these cells was DMEM (Sigma-Aldrich) supplemented with 1x antibiotic/antimycotic (Sigma-Aldrich) and 10% fetal bovine serum (Invitrogen).

siRNA Transfection:

Hela cells were grown in 35mm dishes. The transfection procedure was completed using GeneSilencer Transfection Reagents (Genlantis) by following the manufacturer's instructions. A solution of GeneSilencer reagent and serum free media was mixed for five minutes. A second solution of siRNA diluent, serum free media, and the desired siRNA was also mixed for five minutes. The solutions were then combined and mixed for five minutes. The cells' media was replaced with serum free medium to increase transfection efficiency. Following the addition of the transfection solution, the cells were incubated at 37°C in a humidified environment consisting of 5% CO_2. After 4 hours of incubation, the media was supplemented with serum and the cells were incubated for an additional 48 hours. The following are the siRNA oligonucleotides used throughout the experiments: stathmin1 siRNA 5'-CCCAGUUGAUUGUGCAGAAUU-3' (Thermo Scientific/ Dharmacon) and ITCH siRNA 5'-GAAACUACAUGUUCAGAAA-3' (Thermo Scientific/Dharmacon).

Doxorubicin Treatment:

Doxorubicin is a known DNA damaging agent. It has been shown that treatment of Hela cells with doxorubicin triggers dispersal of the Golgi apparatus (6). In experiments requiring

Golgi dispersal, cells were treated with 25nM of doxorubicin. For knockdown groups, doxorubicin was added 24 hours after the addition of siRNA. Following the addition of doxorubicin, cells were incubated for 24 hours at 37°C in a humidified environment consisting of 5% CO_2.

Immunofluorescence:

Cells were grown on glass coverslips and fixed in -20°C methanol and EDTA (1:200) for 10 minutes. The cells were then rehydrated in PBS and blocked in a phosphate buffered saline (PBS) and fetal bovine serum (FBS; 1:10) for 30 minutes at 37°C. Following block, the cells were incubated with primary antibodies for 45 minutes at 37°C then washed three times in PBS for five-minutes each. This was followed by 45 minutes of incubation with secondary antibodies at 37°C and an additional three five-minutes washes in PBS. Coverslips were mounted onto glass slides using Vectashield (Vector Laboratories). The following is a list of primary antibodies used throughout the experiments: mouse anti-GM130 (1:50; Sigma-Aldrich) to label the Golgi apparatus, rabbit anti-α tubulin (1:100; Sigma-Aldrich) to label microtubules, mouse anti-cleaved PARP (1:50; Sigma-Aldrich) as a marker of apoptosis. The following is a list of secondary antibodies used throughout the experiments: AlexaFluor GAR-488 (1:50; Gibco-Invitrogen), AlexaFluor GAM-568 (1:50; Gibco-Invitrogen), and Propidium Iodide (1:1000; Gibco-Invitrogen) to label DNA. Cells were observed using the 40X objective on an inverted microscope (Nikon TE2000E). Images were acquired using the program MetaVue. For both Golgi dispersal experiments and cleaved PARP experiments at least 50 cells were examined for each group per experiment. Data for cleaved PARP experiments were normalized by setting the

percentage of cleaved PARP positive ITCH depleted cells equal to 1. Normalized data were pooled for cleaved PARP experiments.

Measuring Relative Golgi Area and Statistical Analysis:

Using immunofluorescent images, the relative area of the Golgi was measured. The relative area of the Golgi was manually traced using a selection tool on the program MetaVue. The region statistics provided by MetaVue were used to determine the relative Golgi area (6). Statistical analysis of the collected data was done using unpaired t-tests in Microsoft Excel.

Western Blotting:

Whole cell lysates were prepared using a lysis buffer composed of 2x Hepes/NaCl buffer, protease inhibitor, 200mM EDTA, 10% NP-40, 100mM DTT, 200mM PMSF, and dH_2O. Cells were treated with the lysis buffer on ice for 30 min. Cells were then centrifuged at 13,000rpm for 10 minutes at 4°C. The supernatant was then aspirated and the pellet was discarded. Protein concentrations were measured using a Bradford assay. Lysates were then diluted in SDS PAGE sample buffer and supplemented with β-mercaptoethanol. For each sample, 10μg total protein was loaded per lane and resolved in a 10% polyacrylamide gel. Proteins were then transferred to a PVDF membrane. After transfer, membranes were blocked with 5% nonfat milk in Tris-buffered saline (TBS) with 0.1% Tween. Membranes were then probed using primary antibodies: anti-stathmin (1:2000; Sigma-Aldrich), anti- ITCH (1:1000; GE Healthcare), or anti-α tubulin B512 (1:1000; Sigma-Aldrich) as a loading control. Membranes were then probed using secondary antibodies: goat anti-mouse horseradish peroxidase (1:5000; Sigma- Aldrich) or goat

anti- rabbit horseradish peroxidase (1:5000; Sigma-Aldrich). Immunoreactive bands were developed using enhanced chemiluminscence (ECL) prime (GE Amersham).

Results:

Stathmin depletion in p53-deficient cells has an intermediate effect on Golgi dispersal:

It was hypothesized that stathmin depletion causes stabilization of Golgi nucleated microtubules. Therefore, Golgi dispersal was expected to be slower in stathmin depleted Hela cells compared to control cells. Stathmin depletion was achieved using a siRNA transfection and was confirmed by western blot (Figure 3B). Cells were then treated with the DNA damaging agent doxorubicin to trigger Golgi dispersal. DNA damage via doxorubicin results in the activation of DNA damage activated protein kinase (DNA-PK), which activates the peripheral Golgi protein GOLPH3 by phosphorylation (6). Activated GOLPH3 interacts with the myosin protein MYO18A, which causes actin and myosin interactions to increase the tensile force applied to the Golgi (6). This ultimately causes Golgi fragmentation (6).

In this experimental design there were four conditions: 0 hour doxorubicin treated control, 24 hour doxorubicin treated control, 0 hour doxorubicin treated stathmin depleted, 24 hour doxorubicin treated stathmin depleted. Immunofluorescence was used to label microtubules (anti-α tubulin) and the Golgi apparatus (anti-GM130) (Figure 3A). Microtubules were labeled in order to identify mitotic cells and the position of the centrosome (Figure 3A). The microtubule population was notably denser in stathmin depleted cells (Figure 3A). In untreated cells the Golgi apparatus had a concave shape and was located adjacent to the nucleus and centrosome (Figure 3A). However, in cells that were treated with doxorubicin the Golgi was fragmented and dispersed throughout the cytosol (Figure 3A). Importantly, the Golgi in doxorubicin treated cells

was noticeably more dispersed compared to the Golgi in untreated cells (Figure 3A). For each group, the relative Golgi area was manually traced with a selection tool on the program Metavue. The relative Golgi area was only recorded for cells in interphase.

Data were collected for 594 untreated control cells, 472 untreated stathmin depleted cells, 513 doxorubicin treated control cells, and 458 doxorubicin treated stathmin depleted cells total (Figure 4A & Figure 4B). Unpaired t-tests revealed that there was a significant difference (p-value <0.05) between the doxorubicin treated stathmin depleted cells and the doxorubicin treated control cells, as well as between the untreated stathmin depleted cells and doxorubicin treated stathmin depleted cells (Figure 4A). For further comparison, the average relative Golgi area of the doxorubicin treated control group was considered to be representative of 100% dispersal. Using this as a baseline, the percentage of Golgi dispersal was calculated for the stathmin depleted cells. Doxorubicin treated stathmin depleted cells were on average 64% dispersed. This supports the idea that stathmin depletion in p53-deficient cells has an intermediate effect on Golgi dispersal.

Preliminary evidence that stathmin depletion results in increased activity of ITCH:

Immunofluoresence was used to label DNA (propidium iodide) and cleaved PARP (anti-cl-PARP) in Hela cells. During apoptosis, the executioner caspase, caspase 3, has the dual function of cleaving poly ADP ribose polymerase (PARP) and releasing caspase-dependent DNase (CAD) from its inhibitor iCAD. Active CAD enters the nucleus and works with cleaved PARP to degrade DNA and ultimately cause cell death (5). Thus, cleaved PARP was labeled as a marker for apoptosis (5).

In this experimental design there were four groups: untreated, stathmin depleted, ITCH depleted, and stathmin/ITCH depleted. Stathmin and ITCH depletion was achieved using siRNA transfections and was confirmed by western blot (Figure 5B). Cells that were positive for cleaved PARP were considered apoptotic. It was predicted that ITCH knockdown would restore cell viability in stathmin depleted cells. Therefore, it was expected that there would be a higher percentage of death among stathmin depleted cells compared to stathmin/ITCH double depleted cells.

Data were normalized against the percentage of cleaved PARP positive ITCH depleted cells and pooled for all experiments. We found a lower percentage of cleaved PARP positive cells in the stathmin/ITCH double depleted group compared the stathmin depleted group (Figure 5A). This is preliminary evidence that ITCH knockdown restores cell viability in stathmin depleted cells.

Discussion:

Stathmin is a microtubule destabilizing protein that is overexpressed in some highly malignant cancer cells (1). The role of stathmin in cancer cell fate has been documented within the literature. Specifically, stathmin depletion in p53-deficient cells causes a ~4 hour delay in mitotic entry and an increase in cell death via the extrinsic apoptotic pathway (11; 12). In this work we explored two independent models that we predicted were responsible for the delay in mitotic entry and increase in cell death, respectively.

The first model suggested that stathmin acts on Golgi nucleated microtubules. We hypothesized that stathmin depletion would stabilize Golgi nucleated microtubules and slow Golgi dispersal, thus delaying mitotic entry. To test this model we triggered Golgi dispersal in

stathmin depleted p53-deficient cells. We demonstrated that there is a significant difference in Golgi dispersal between doxorubicin treated control cells and doxorubicin treated stathmin depleted cells. Specifically, Golgi dispersal in doxorubicin treated stathmin depleted cells was approximately 64% that of control cells. This suggests that stathmin depletion has an intermediate effect on Golgi dispersal. Other work in the lab has shown that there is no significant change in the stability of Golgi microtubules in stathmin depleted p53-deficient cells compared to control cells (8). Therefore, we conclude that there is not strong evidence for stathmin depletion working via Golgi stabilization. It is possible that our finding is an artifact of a different pathway initiated by the doxorubicin treatment.

The second model suggested that stathmin depletion works through a negative feedback loop to promote cell death via the extrinsic apoptotic pathway. Our model suggests that stathmin depletion results in prolonged activation of JNK causing phosphorylation of the E3 ubiquitin ligase ITCH, and subsequent degradation of c-FLIP, a protein that blocks caspase 8 activation. Therefore, we predicted that stathmin depletion induces apoptosis by increasing the amount of activated ITCH. To test this model we labeled cleaved-PARP in stathmin/ITCH double depleted p53-deficient cells as a marker for apoptosis. We found preliminary evidence that ITCH knockdown restores cell viability in stathmin depleted p53-deficient cells. However, additional research is necessary to confirm this link. Future research will consist of additional cleaved PARP experiments and live-cell imaging to track cell death in stathmin/ITCH double depleted p53-deficient cells. It is also essential to confirm that stathmin depletion results in an increase in phosphorylated ITCH due to prolonged JNK activation. Confirmation of this signaling pathway would identify a specific mechanism by which stathmin depletion results in the activation of the extrinsic apoptotic pathway in p53-deficient cells.

In conclusion, the link between microtubule regulation and decisions regarding cell fate is intricate. Evidence supports that stathmin has a unique role in promoting cell survival in some forms of cancer. It has been shown that stathmin depletion in p53-deficient cells delays mitotic entry and results in an increase in cell death (11; 12). In this work we have ruled out the possibility of stathmin depletion causing a delay in mitotic entry by slowing dispersal of the Golgi ribbon. Further, we have preliminary support for stathmin depletion causing an increase in cell death through a signal transduction pathway with ITCH. Identifying the specific mechanisms by which stathmin depletion effects p53-deficient cells continues to be an active area of research. Further characterization of stathmin can prove to be influential in the development of cancer therapies.

A.

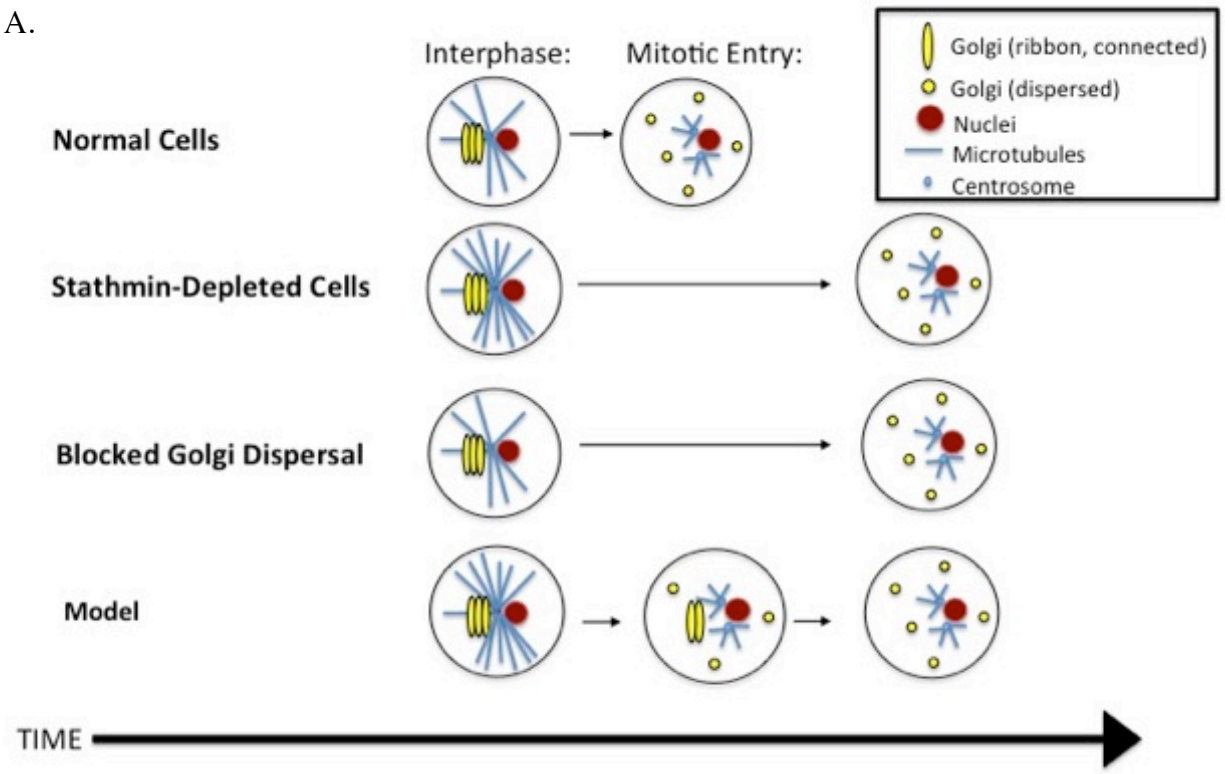

Figure 1: Known Phenotypes and Proposed Model for Cell Cycle Delay in Stathmin Depleted p53-Deficient Cells. A. Normally, p53-deficient cells enter mitosis at some point in time. Mitotic entry is delayed by ~4 hours in stathmin depleted p53-deficient cells (11). Similarly, mitotic entry is delayed when Golgi dispersal is blocked (14). We propose that these two phenotypes are linked. We predict that stathmin depletion in p53-deficient cells stabilizes Golgi nucleated microtubules, thus slowing Golgi fragmentation and subsequently delaying mitotic entry.

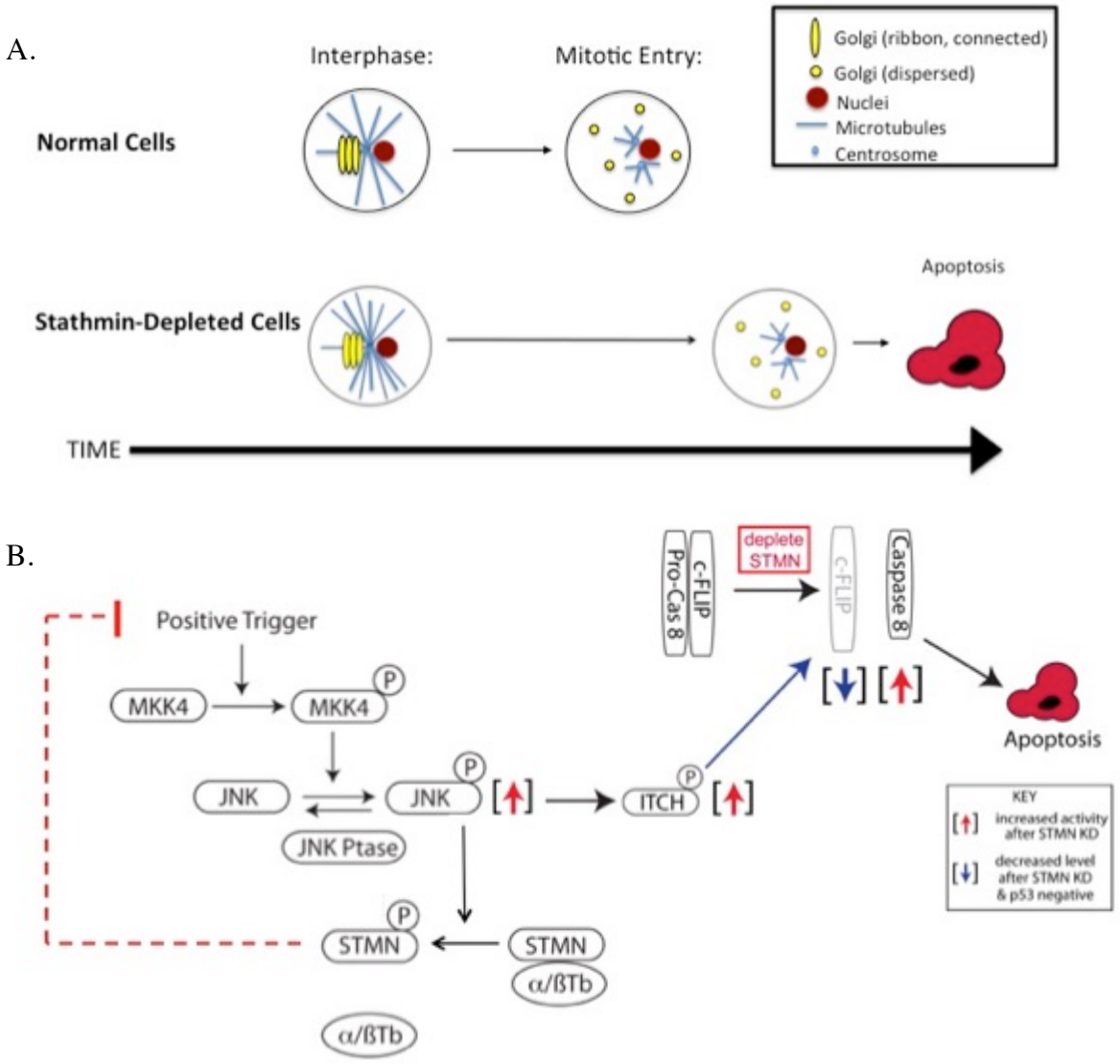

Figure 2: A. Phenotype of Stathmin Depleted p53-Deficient Cells. In stathmin depleted p53-deficient cells mitotic entry is delayed and there is an increase in cell death. **B. Proposed Model for Increased Cell Death in Stathmin Depleted p53-deficient Cells.** A positive trigger activates MKK4 through phosphorylation. Phosphorylated MKK4 activates JNK. JNK inactivates stathmin through phosphorylation. Phosphorylated stathmin is involved in a negative feedback loop that inhibits the activation of MKK4. We propose stathmin depletion results in prolonged activation of JNK, which in turn causes the activation of the E3 ubiquitin ligase ITCH. Activated ITCH subsequently ubiquinates c-FLIP, which causes its degradation. The degradation of c-FLIP promotes the activation of caspase 8 and cell death via the extrinsic apoptotic pathway.

A.

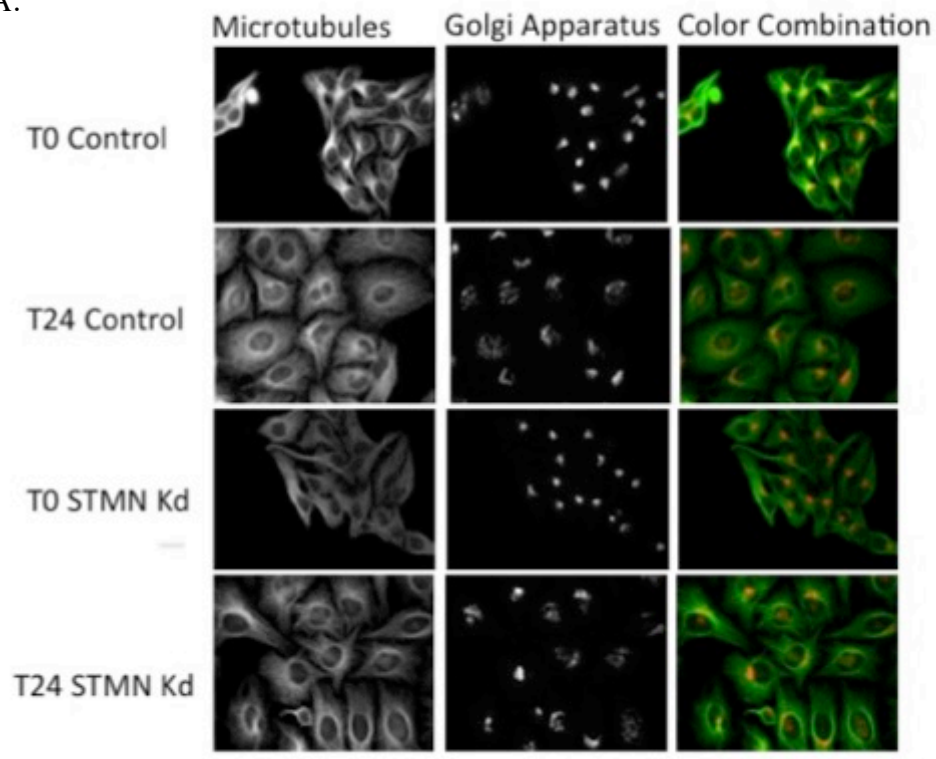

B.

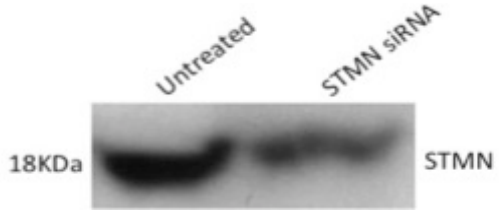

Figure 3: A. Immunofluorescent Images of Microtubules and the Golgi Apparatus in Hela Cells. Microtubules were stained using the primary antibody rabbit anti-α tubulin (1:100) and the secondary antibody AlexaFluor GAR-488. The Golgi apparatus was stained using the primary antibody mouse anti-GM130 (1:50) and the secondary antibody AlexaFluor GAM-568 (1:50). In order from left to right the columns correspond to images of microtubules, the Golgi apparatus, and a color combination that overlays the two. From top to bottom the rows correspond to an untreated control group, a doxorubicin treated control group, an untreated stathmin depleted group, and a doxorubicin treated stathmin depleted group. Cells in the doxorubicin treated groups were treated with 25nM of doxorubicin for 24 hours. **B. Western Blot.** Western blot confirms successful knockdown of stathmin. Stathmin has a molecular weight of 18KDa.

A.

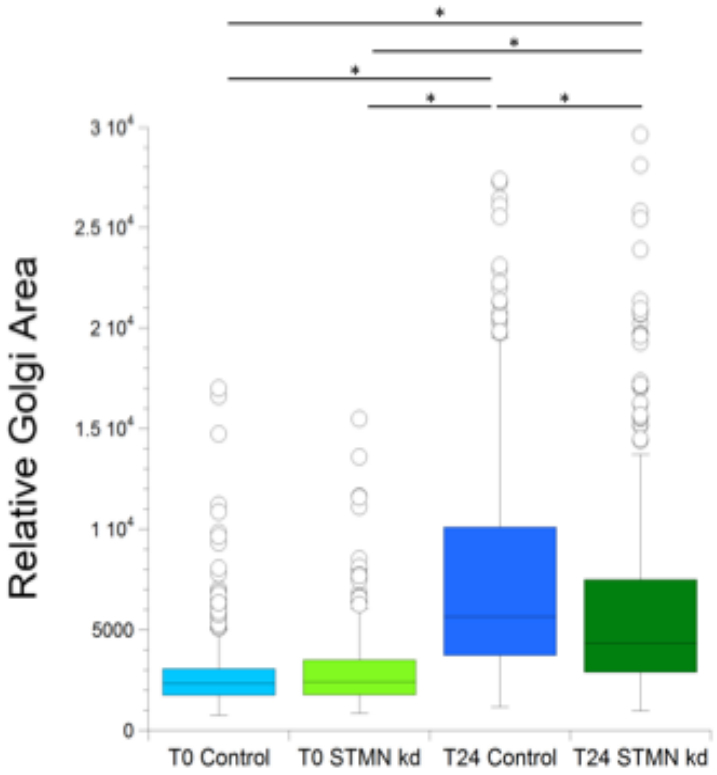

B.

	Average Relative Golgi Area (Arbitrary Units)
T0 Control	2687.0
T24 Control	7548.7
T0 STMN kd	2884.3
T24 STMN kd	6010.7

Figure 4: A. Relative Golgi Area. The relative Golgi area was measured by manually tracing the area of the Golgi using the program MetaVue. The results were plotted using the program Kaleidagraph. Statistical significance was determined using unpaired t-tests on Microsoft Excel. A p-value < 0.05 was considered significant. Statistical significance is indicated by a (*), which corresponds to a p-value < 0.001. The only relationship that was not statistically significant was between the untreated control group and the untreated stathmin depleted group where $p= 0.058$.

B. Average Relative Golgi Area. Average relative Golgi area listed for each group.

A.

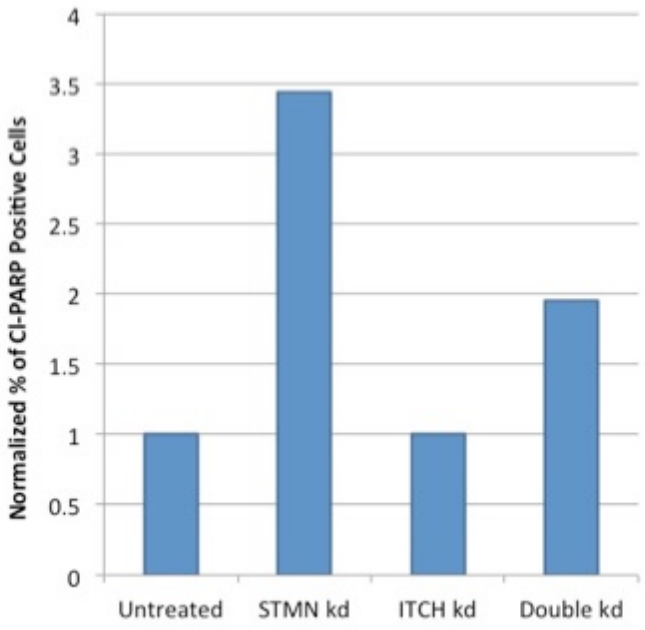

B.

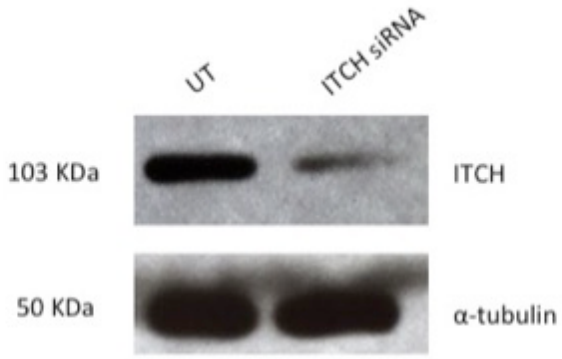

Figure 5: A. Normalized Percentage of Cleaved-PARP Positive Cells. The nucleus was stained using propidium iodide (1:1000). Cleaved-PARP was stained using the primary antibody mouse anti-cleaved PARP (1:50) and the secondary antibody AlexaFluor GAM-568 (1:50). Cleaved-PARP positive cells were counted. This experiment was completed twice. Data were normalized and compiled. The results were graphed using Microsoft Excel. **B. Western Blot.** Western blot confirms successful knockdown of ITCH. ITCH has a molecular weight of 103KDa. The blot was also probed for α-tubulin as a loading control. Tubulin has a molecular weight of 50KDa.

References

1) Carney, B. K., & Cassimeris, L. (2010). Stathmin/Oncoprotein 18, A microtubule regulatory protein, is required for survival of both normal and cancer cell lines lacking the tumor suppressor, p53. *Cancer Biology and Therapy, 9*(9), 699-709. doi:10.4161/cbt.9.9.11430

2) Cassimeris, L., Lingappa, V. R., & Plopper, G. (2010). *Cells* (Second ed.) Jones & Bartlett Learning.

3) Chang, L., Kamata, H., Solinas, G., Luo, J., Maeda, S., Venuprasad, K., Liu, Y., & Karin, M. (2006). The E3 ubiquitin ligase itch couples JNK activation to TNFα- induced cell death by inducing c-$FLIP_L$ Turnover. *Cell, 124*(3), 601-613. doi:10.1016/j.cell.2006.01.021

4) Colanzi, A., & Corda, D. (2007). Mitosis controls the golgi and the golgi controls mitosis. *Current Opinion in Cell Biology, 19*, 386-393. doi:10.1016/j.ceb.2007.06.002

5) Elmore, S. (2007). Apoptosis: A review of programmed cell death. *Toxicology and Pathology, 35*(4), 495-516.

6) Farber-Katz, S. E., Dippold, H. C., Buschman, M. D., Peterman, M. C., Xiang, M., Noakes, C. J., Tat, J., Ng, M. M., Rahajeng, J., Cowan, D. M., Fuchs, G. J., Zhou, H., & Field, S. J. (2014). DNA damage triggers golgi disperal via DNA-PK and GOLPH3. *Cell, 156*(3), 413-427. doi:10.1016/j.cell.2013.12.023

7) Persico, A., Cervigni, R. I., Barretta, M. L., Corda, D., & Colanzi, A. (2010). Golgi partitioning controls mitotic entry through aurora-A kinase. *Molecular Biology of the Cell, 21*, 3708-3721. doi:10.1091/mbc.E10-03-0243

8) Peters, K., & Cassimeris, L. (Unpublished Lehigh University)

9) Rios, R. M. (2014). The centrosome-- golgi apparatus nexus. *Philisophical Transactions of the Royal Society, 369*, 1-9.

10) Rivero, S., Cardenas, J., Bornens, M., & Rios, R. M. (2009). Microtubule nucleation at the cis- side of the golgi apparatus requires AKAP450 and GM130. *The EMBO Journal, 28*(8), 1016-1028. doi:10.1038/emboj.2009.47

11) Silva, V. C., & Cassimeris, L. (2013). Stathmin and microtubules regulate mitotic entry in HeLa cells by controlling activation of both aurora kinase A and Plk1. *Molecular Biology of the Cell, 24*(24), 3919-3931. doi:10.1091/mbc.E13-02-0108

12) Silva, V. C., Plooster, M., Leung, J. C., & Cassimeris, L. (2015). A delay prior to mitotic entry triggers caspase 8- dependent cell death in p53-deficient hela and HCT-116 cells. *Cell Cycle, 14*(7), 1070-1081. doi:10.1080/15384101.2015.1007781

13) Sutterlin, C., & Colanzi, A. (2010). The golgi and the centrosome: Building a functional partnership. *Journal of Cell Biology, 188*(5), 621-628. doi:10.1083/jcb.200910001

14) Sutterlin, C., Hsu, P., Mallabiabarrena, A., & Malhotra, V. (2002). Fragmentation and dispersal of the pericentriolar golgi complex is required for entry into mitosis in mammalian cells. *Cell, 109*(3), 359-369. doi:10.1016/S0092-8674(02)00720-1

15) Zhao, E., Amir, M., Lin, Y., & Czaja, M. J. (2014). Stathmin mediates hepatocyte resistance to death from oxidative stress by down regulating JNK. *PLoS One, 9*(10), 1-12. doi:10.1371/journal.pone.0109750